DFIG Sliding Mode Control Driven by Wind Turbine with Using a SVM Inverter for Improve the Quality of Energy Injected into the Electrical Grid

Youcef Bekakra[1] and **Djilani Ben Attous**[2], Non-members

ABSTRACT

This paper presents a simulation study of Doubly Fed Induction Generator (DFIG) controlled by sliding mode control (SMC) applied to achieve control of active and reactive powers exchanged between the stator of the DFIG and the grid. In this paper, a variable speed wind turbine is considered with DFIG and different power electronic converter topologies: (i) Carried based Pulse Width Modulation (PWM), (ii) Space Vector Modulation (SVM). To improve the quality of energy injected into the electrical grid, we propose SVM technique which allows the minimizing of harmonics stator current and wide linear modulation range. The feasibility and effectiveness of the method is demonstrated by simulation results. The obtained results showed that, the proposed SMC with SVM inverter have stator and rotor current with low harmonic distortion and low active and reactive powers ripples than PWM inverter.

Keywords: Doubly fed induction generator, Wind turbine, Sliding mode control, Space vector modulation, Pulse width modulation.

1. INTRODUCTION

Wind energy is becoming one of the most important renewable energy sources. Recently, power converter control has mostly been studied and developed for wind energy conversion system (WECS) integration in the electrical grid. The use of power electronic converters allows variable speed operation of the wind turbine where the WECS extracts maximum power from the turbine [1].

One of the generation systems commercially available in the wind energy market currently is the doubly fed induction generator (DFIG) with its stator winding directly connected to the grid and with its rotor winding connected to the grid through a variable frequency converter as shown in Fig. 1. One of the most advantages of this system is that the rating of the power converter is one third of that of the generator [2]. Vector control technology is used to control the generator, and the rotor of DFIG is connected to an AC excitation of which the frequency, phase, and magnitude can be adjusted. Therefore, constant operating frequency can be achieved at variable wind speeds [3]. The variable speed constant frequency wind power generation is mainly based on the research of optimal power-speed curve, namely the most mechanical power of turbine can be achieved by regulating the speed of generator, where the wind speed may be detected or not [3]. The paper adopts the vector transformation control method of stator-oriented magnetic field to realize the decoupling control for the stator active and reactive power using sliding mode control (SMC). Sliding mode theory, stemmed from the variable structure control family, has been used for the induction motor drive for a long time. It has for long been known for its capabilities in accounting for modelling imprecision and bounded disturbances. It achieves robust control by adding a discontinuous control signal across the sliding surface, satisfying the sliding condition [4]. The power quality problems, such as large values of harmonics, poor power factor and high total harmonic distortion, are usually associated with operation of three-phase AC/DC converters. Negative effects of harmonics, such as failures in computer operation and data transmission, high noise levels in telephone communications, malfunction of sensitive electronic equipment, resonance

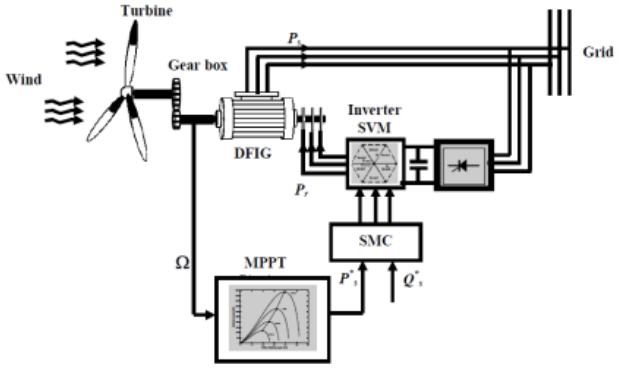

Fig. 1: *Schematic diagram of DFIG-based wind generation systems.*

Manuscript received on April 10, 2013 ; revised on May 12, 2013.

[1,2] The authors are with Department of Electrical Engineering, Faculty of Sciences and Technology, University of El Oued., E-mail: youcef1984@gmail.com and dbenattous@yahoo.com

conditions in power supply network, aging of insulation and additional losses in electrical machines, capacitive bank failures and so on, are well known. To diminish these effects, many countries have issued harmonics limitation standards or recommendations [5]. Traditionally the sinusoidal pulse-width modulation (SPWM) technique is widely used in variable speed drive of induction machine, especially for scalar control where the stator voltage and frequency can be controlled with minimum online computational requirement. In addition, this technique is easy to implement. However, this algorithm has the following drawbacks. This technique is unable to fully utilize the available DC bus supply voltage to the voltage source inverter. This technique gives more total harmonic distortion (THD), this algorithm does not smooth the progress of future development of vector control implementation of AC drive. These drawbacks lead to development of a sophisticated PWM algorithm which is Space Vector Modulation (SVM). This algorithm gives 15% more voltage output compare to the sinusoidal PWM algorithm, thereby increasing the DC bus utilization. Furthermore, it minimizes the THD as well as loss due to minimize number of commutations in the inverter [6]. In this paper, we apply the SMC method to the DFIG based on wind energy using the modulation strategy known as SVM technique and compared with the traditional PWM technique.

2. MODELING OF THE WIND GENERATOR

The aerodynamic power, which is converted by a wind turbine, P_t is dependent on the power coefficient C_p. It is given by [7]:

$$P_t = \frac{1}{2} C_p \rho \pi R^2 V^3 \tag{1}$$

where ρ is the air density, R is the blade length and is the wind speed. The turbine torque is the ratio of the output power to the shaft speed Ω_t:

$$C_t = \frac{P_t}{\Omega_t} \tag{2}$$

The turbine is normally coupled to the generator shaft through a gear box whose gear ratio is chosen in order to set the generator shaft speed within a desired speed range. Neglecting the transmission losses, the torque and shaft speed of the wind turbine, referred to the generator side of the gear box, are given by:

$$C_g = \frac{C_t}{G} \text{ and } \Omega_t = \frac{\Omega_{mec}}{G} \tag{3}$$

Where Ω_{mec} is the generator shaft speed. A wind turbine can only convert just a certain percentage of the captured wind power. This percentage is represented by $C_p(\beta, \lambda)$ which is function of the wind speed, the turbine speed and the pith angle of specific wind turbine blades. Although this equation seems simple, C_p is dependent on the ratio λ between the turbine angular velocity Ω_t and the wind speed v. This ratio is called the tip speed ratio:

$$\lambda = \frac{\Omega_t \cdot R}{v} \tag{4}$$

C_p can be described as [8]:

$$C_p(\beta, \lambda) = (0.5 - 0.0167(\beta - 2)) \sin \frac{\pi(\lambda + 0.1)}{18.5 - 0.3(\beta - 2)} - 0.00184(\lambda - 3)(\beta - 2) \tag{5}$$

A typical relationship between C_p, β and λ is shown in Fig.2. It is clear from this figure that there is a value of λ for which C_p is maximum and that maximize the power for a given wind speed. The peak power for each wind speed occurs at the point where C_p is maximized. To maximize the generated power, it is therefore desirable for the generator to have a power characteristic that will follow the maximum C_{p_max} line. The maximum value of C_p (C_{p_max}=0.5) is achieved for $\beta = 2$ degree and for $\lambda_{opt} = 9.2$.

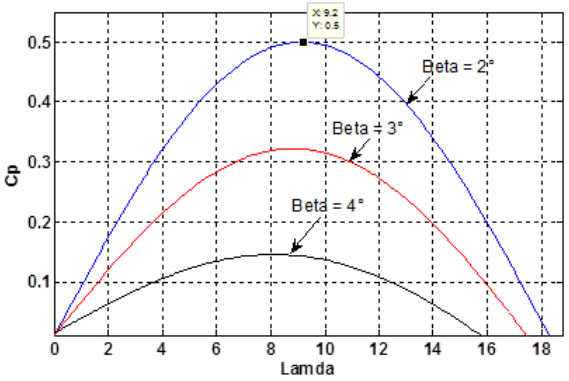

Fig.2: *Aerodynamic power coefficient variation C_p against tip speed ratio λ and pitch angle β.*

To extract the maximum power generated, we must fix the advance report λ_{opt} and the maximum power coefficient C_{p_max}. An estimate of wind speed value can be obtained [9]:

$$v_{est} = \frac{R \cdot \Omega_t}{\lambda_{opt}} \tag{6}$$

The reference mechanical power value must be set to the following value [9]:

$$P_{m\_ref} = \frac{1}{2} \frac{C_{p\_max}}{\lambda_{opt}^3} \cdot \rho \cdot \pi \cdot R^5 \cdot \frac{\Omega_{mec}^3}{G^3} \tag{7}$$

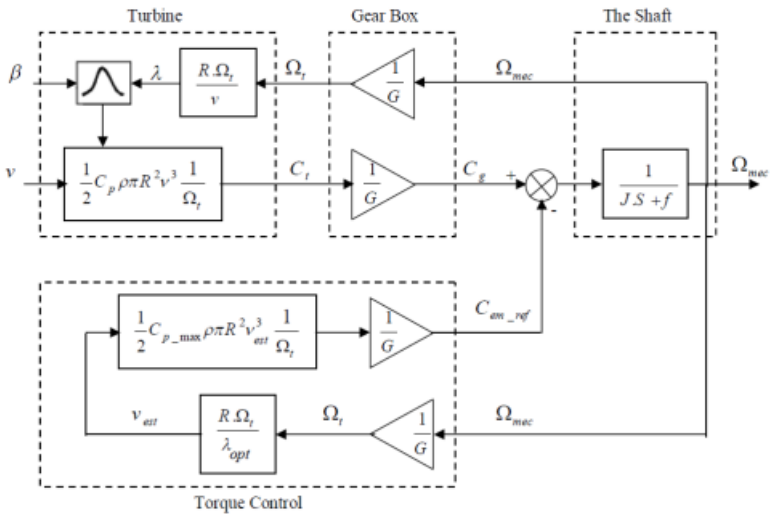

Fig.3: *Wind turbine model with torque control.*

The electromagnetic torque reference value also must be set to the following value:

$$C_{em\_ref} = \frac{P_{m\_ref}}{\Omega_t} = \frac{1}{2}\frac{C_{p\_max}}{\lambda_{opt}^3} \cdot \rho \cdot \pi \cdot R^5 \cdot \frac{\Omega_{mec}^3}{G^3} \quad (8)$$

The simplified representation of wind turbine model with torque control in the form of diagram blocks is given in Fig.3. Fig. 4 shows the turbine mechanical powers various speed characteristics for different wind speeds, with indication of the maximum power point tracking (MPPT) curve.

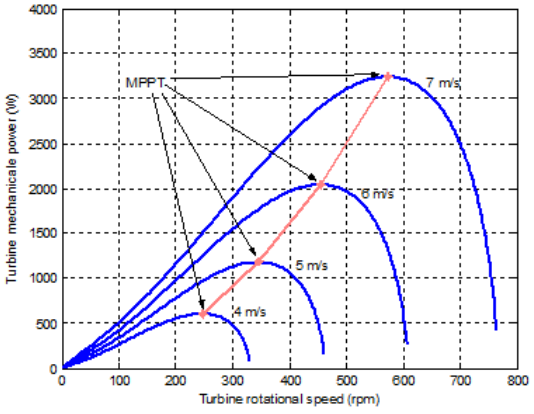

Fig.4: *Turbine powers various speed characteristics for different wind speeds, with indication of the maximum power point tracking (MPPT) curve.*

3. DFIG MODELS

The general electrical state model of the induction machine obtained using Park transformation is given by the following equations [10]: Stator and rotor voltages:

$$\begin{cases} V_{sd} = R_s \cdot i_{sd} + \frac{d}{dt}\phi_{sd} - \omega_s \cdot \phi_{sq} \\ V_{sq} = R_s \cdot i_{sq} + \frac{d}{dt}\phi_{sq} + \omega_s \cdot \phi_{sd} \\ V_{rd} = R_r \cdot i_{rd} + \frac{d}{dt}\phi_{rd} - (\omega_s - \omega) \cdot \phi_{rq} \\ V_{rq} = R_r \cdot i_{rq} + \frac{d}{dt}\phi_{rq} + (\omega_s - \omega) \cdot \phi_{rd} \end{cases} \quad (9)$$

Stator and rotor fluxes:

$$\begin{cases} \phi_{sd} = L_s \cdot i_{sd} + M \cdot i_{rd} \\ \phi_{sq} = L_s \cdot i_{sq} + M \cdot i_{rq} \\ \phi_{rd} = L_r \cdot i_{rd} + M \cdot i_{sd} \\ \phi_{rq} = L_r \cdot i_{rq} + M \cdot i_{sq} \end{cases} \quad (10)$$

The active and reactive powers at the stator and the rotor as well as those provide for grid are defined as:

$$\begin{cases} P_{sd} = V_{sd} \cdot i_{sd} + V_{sq} \cdot i_{sq} \\ Q_{sd} = V_{sq} \cdot i_{sd} - V_{sd} \cdot i_{sq} \end{cases} \quad (11)$$

$$\begin{cases} P_{rd} = V_{rd} \cdot i_{rd} + V_{rq} \cdot i_{rq} \\ Q_{rd} = V_{rq} \cdot i_{rd} - V_{rd} \cdot i_{rq} \end{cases} \quad (12)$$

The electromagnetic torque is done as:

$$C_e = P\frac{M}{L_s}(\phi_{sd} i_{rq} - \phi_{sq} i_{rd}) \quad (13)$$

and its associated motion equation is:

$$C_e - C_r = J\frac{d\omega}{dt} \quad (14)$$

4. SPACE VECTOR MODULATION

The SVM method considers this interaction of the phase and optimizes the harmonic content of the three phase isolated neutral load as shown in Fig. 5, [11]. The three phase sinusoidal and balance voltages

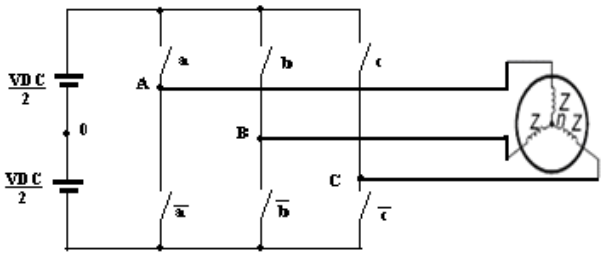

Fig.5: *Voltage source inverter type 3 phase.*

given by the equations as follows:

$$\begin{cases} V_{An} = V_m \cos \omega t \\ V_{Bn} = V_m \cos(\omega t - \frac{2\pi}{3}) \\ V_{Cn} = V_m \cos(\omega t + \frac{2\pi}{3}) \end{cases} \quad (15)$$

$$V^- = \frac{2}{3}[V_{An} + aV_{Bn} + a^2 \cdot V_{Cn}] \quad (16)$$

Are applied to the three phase DFIG, using (16). A three phase bridge inverter, from Fig. 5, has 8 permissible switching states. Table I gives summary of the switching states and the corresponding phase-to-neutral voltage of isolated neutral machine.

$$V_{no} = \frac{1}{2} median(V_{An}, V_{Bn}, V_{Cn}) \quad (17)$$

Double edge modulation of reference voltage V_{An},V_{Bn},and V_{Cn} are equal as follows:

$$\begin{cases} V_{Ao} = V_{An} + V_{no} \\ V_{Bo} = V_{Bn} + V_{no} \\ V_{Co} = V_{Cn} + V_{no} \end{cases} \quad (18)$$

The underlying theory behind SVM is to apply space

Table 1: *Summary of inverter switching states.*

Name	A	B	C	V_{An}	V_{Bn}	V_{Cn}
V_0	0	0	0	0	0	0
V_1	1	0	0	$2V_{DC}/3$	$-V_{DC}/3$	$-V_{DC}/3$
V_2	1	1	0	$V_{DC}/3$	$V_{DC}/3$	$-2V_{DC}/3$
V_3	0	1	0	$-V_{DC}/3$	$2V_{DC}/3$	$-V_{DC}/3$
V_4	0	1	1	$-2V_{DC}/3$	$V_{DC}/3$	$V_{DC}/3$
V_5	0	0	1	$-V_{DC}/3$	$-V_{DC}/3$	$2V_{DC}/3$
V_6	1	0	1	$V_{DC}/3$	$-2V_{DC}/3$	$V_{DC}/3$
V_7	1	1	1	0	0	0

vectors as illustrated in Fig. 6 for varying time periods in a pattern based on the SVM algorithm.

4.1 The SVM generator

The SVM generator, whose operating principle is presented in Fig. 7, contains seven blocks with the following functions [12]:

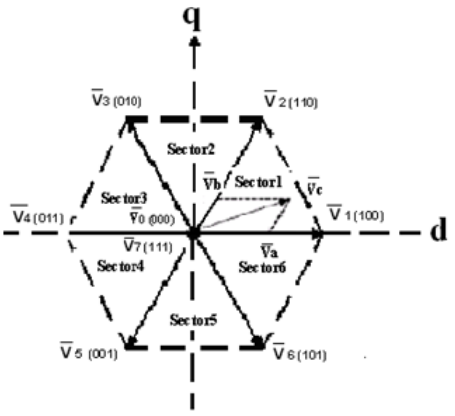

Fig.6: *Space vector of voltage.*

- The three-phase generator is used to produce three sine waves with variable frequency and amplitude; the three signals are out of phase with each other by 120°.
- The low-pass bus filter is used to remove fast transients from the DC bus voltage measurement; this measure is used to compute the voltage vector applied to the machine.
- The $\alpha\beta$ transformation converts variables from the three-phase system to the two-phase $\alpha\beta$ system.
- The $\alpha\beta$ vector sector is used to find the sector of the $\alpha\beta$ plane in which the voltage vector lies; this plane is divided into six different sectors spaced by 60°.
- The ramp generator is used to produce a unitary ramp at the PWM switching frequency; this ramp is used as a time base for the switching sequence.
- The switching time calculator is used to calculate the timing of the voltage vector applied to the machine.
- The gates logic compares the ramp and the gate timing signals to activate the inverter switches at the proper time.

4.2 The simulation in Matlab/Simulink of the SVM generator

The Simulink scheme of SVM generator is presented in Fig.8, the presentation in detail with the simulation of the component blocks in Matlab/Simulink and the analyzing of the main signals is done in [13].

5. ACTIVE AND REACTIVE DFIG INDIRECT POWER CONTROL

A dâĂŞq reference frame synchronized with the stator flux is employed. By setting the quadratic component of the stator to the null value as follows [7]:

$$\phi_{sd} = \phi_s \text{ and } \phi_{sq} = 0 \quad (19)$$

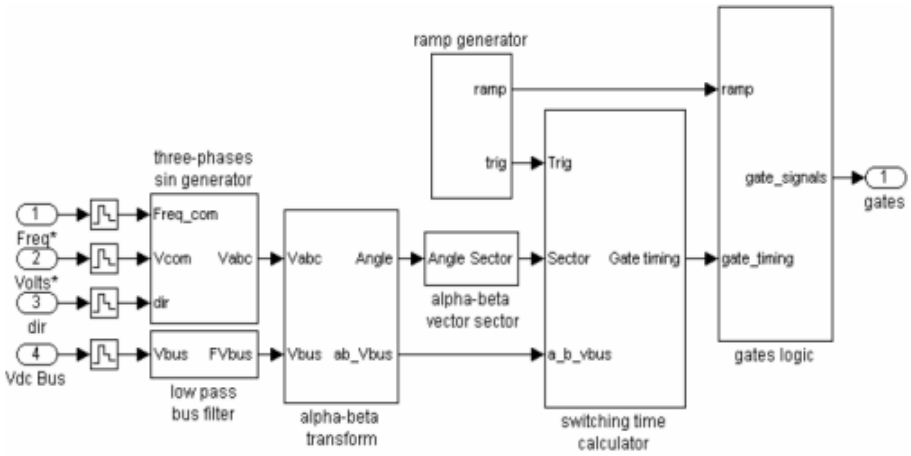

Fig.8: *The Simulink scheme of SVM generator.*

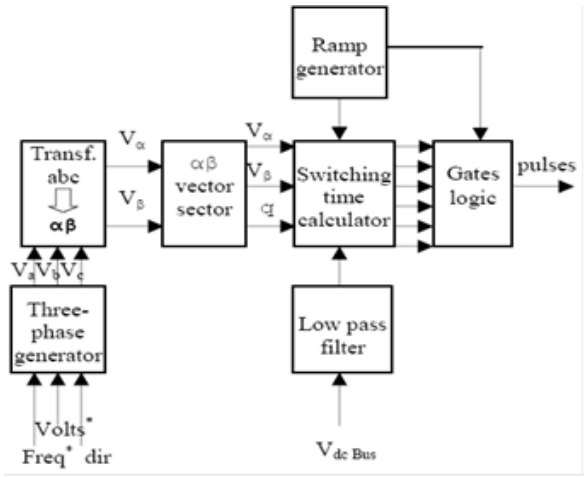

Fig.7: *The operating principle of the inverter SVM.*

Then the torque is simplified as indicated below:

$$C_e = P\frac{M}{L_s} i_{rq} \cdot \phi_{sd} \tag{20}$$

The electromagnetic torque, and subsequently the active power; will only depend on the rotor current along the q-axis. By neglecting the stator resistance R_s, (9) gives:

$$V_{sd} = 0 \text{ and } V_{sq} = V_s \tag{21}$$

In order to calculate angles for the Park transformation for stator and rotor variables, the stator pulsation and the mechanical speed must be sensed.

By choosing this reference frame, stator voltages and fluxes can be rewritten as follows:

$$\begin{cases} V_{sd} = 0 \; ; V_{sq} = V_s = \omega_S \cdot \phi_{sd} \\ \phi_{sd} = \phi_s = L_s \cdot i_{sd} + M \cdot i_{rd} \; ; \\ \phi_{rd} = L_r \cdot i_{rd} + M \cdot i_{sd} \\ \phi_{sq} = 0 = L_s \cdot i_{sq} + M \cdot i_{rq} \; ; \\ \phi_{rq} = L_r \cdot i_{rq} + M \cdot i_{sq} \end{cases} \tag{22}$$

The stator active and reactive power can be written according to the rotor currents as:

$$P_s = -V_s \frac{M}{L_s} i_{rq} \tag{23}$$

$$Q_s = \frac{V_s^2}{\omega_s L_s} - V_s \frac{M}{L_s} i_{rd} \tag{24}$$

The arrangement of the equations gives the expressions of the rotor voltages according to the rotor currents:

$$\dot{i}_r d = -\frac{1}{\sigma T_r} i_{rd} + g\omega_s i_r g + \frac{1}{\sigma L_r} V_{rd} \tag{25}$$

$$\begin{aligned} \dot{i}_{rg} = &-\frac{1}{\sigma}\Big(\frac{1}{T_r} + \frac{M^2}{L_s T_s L_r}\Big) i_{rg} - g\omega_s i_{rd} \\ &+ \frac{1}{\sigma L_r} V_{rq} \end{aligned} \tag{26}$$

with

$$\sigma = 1 - \frac{M^2}{L_s \cdot L_r}; T_r = \frac{L_r}{R_r}; g = \frac{\omega_s - \omega}{\omega_s}; T_s = \frac{L_s}{R_s}$$

6. SLIDING MODE CONTROLLER

A Sliding Mode Controller (SMC) is a Variable Structure Controller (VSC). Basically, a VSC includes several different continuous functions that can map plant state to a control surface, whereas switching among different functions is determined by plant state represented by a switching function [14].

The design of the control system will be demonstrated for a following nonlinear system [15]:

$$\dot{x} = f(x, y) + B(x, t) \cdot u(x, t) \tag{27}$$

Where $x \in \Re^n$ is the state vector, $f(x,t) \in \Re^n$, $B(x,t) \in \Re^{n \times m}$, $u \in \Re^m$ is the control vector. From the system (27), it possible to define a set S of the state trajectories such as:

$$S = \{x(t) | \sigma_s(x, t) = 0\} \tag{28}$$

Where

$$\sigma_s(x,t) = [\sigma_{s1}(x,t), \sigma_{s2}(x,t), ..., \sigma(x,t)]^T \quad (29)$$

and $[.]^T$ denotes the transposed vector, S is called the sliding surface. To bring the state variable to the sliding surfaces, the following two conditions have to be satisfied:

$$\sigma_s(x,t) = 0, \dot{\sigma}_s(x,t) = 0 \quad (30)$$

The control law satisfies the precedent conditions is presented in the following form:

$$\begin{cases} u = u^{eq} + U^n \\ u^n = -k_f sgn(\sigma_s(x,t)) \end{cases} \quad (31)$$

Where u is the control vector, u^{eq} is the equivalent control vector, u^n is the switching part of the control (the correction factor), k_f is the controller gain. u^{eq} can be obtained by considering the condition for the sliding regimen, $\sigma_s(x,t) = 0$. The equivalent control keeps the state variable on sliding surface, once they reach it. For a defined function φ [16], [17], as shown in Fig.9:

$$sgn(\varphi) = \begin{cases} 1, & if\ \varphi > 0 \\ 0, & if\ \varphi = 0 \\ -1, & if\ \varphi < 0 \end{cases} \quad (32)$$

The controller described by the equation (31)

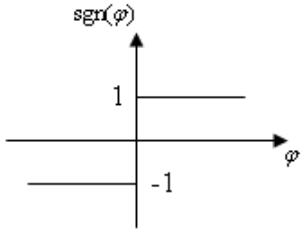

Fig.9: *Sgn function.*

presents high robustness, insensitive to parameter fluctuations and disturbances, but it will have high-frequency switching (chattering phenomena) near the sliding surface due to function involved. These drastic changes of input can be avoided by introducing a boundary layer with width ϵ [15]. Thus replacing $sgn(\sigma_s(x,t))$ by $sat(\sigma_s(x,t))$ (saturation function), in (31), we have:

$$u = u^{eq} - k_f sat(\sigma_s(x,t)) \quad (33)$$

Where $\epsilon > 0$:

$$sat(\varphi) = \begin{cases} sgn(\varphi), & if\ |\varphi| \geqslant \epsilon \\ \varphi, & if\ \ \varphi < \epsilon \end{cases} \quad (34)$$

Fig.10 shows the saturation function. Consider a Lyapunov function [16]:

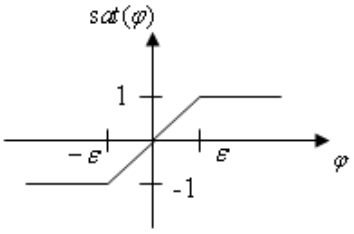

Fig.10: *Saturation function.*

$$V = \frac{1}{2}\sigma_s^2 \quad (35)$$

From Lyapunov theorem we know that if $\dot{V}$ is negative definite, the system trajectory will be driven and attracted toward the sliding surface and remain sliding on it until the origin is reached asymptotically [15]:

$$\dot{V} = \frac{1}{2}\frac{d}{dt}\sigma_s^2 = \sigma_s\dot{\sigma}_s \leqslant -\eta|\sigma_s| \quad (36)$$

Where η is a strictly positive constant.

In this paper, we use the sliding surface proposed par J.J. Slotine,

$$\sigma_s(x,t) = \left(\frac{d}{dt} + \tau\right)^{n-1} e \quad (37)$$

Where: $x = [x, \dot{x}, ..., x^{n-1}]^T$ is the state vector, $x_d = [x_d, \dot{x_d}, ..., x_d^{n-1}]^T$ is the desired state vector, $e = x_d - x = [e, \dot{e}, ..., e^{n-1}]^T$ is the error vector, and τ is a positive coefficient, and n is the system order.

Commonly, in doubly fed induction machine (DFIM) control using sliding mode theory, the surfaces are chosen as functions of the error between the reference input signal and the measured signals [15].

7. APPLICATION OF SLIDING MODE CONTROL TO DFIG

The rotor currents i_{rq} and i_{rd} are the images respectively of stator active power P_s and stator reactive power Q_s have to track appropriate current references, so, a sliding mode control based on the above Park reference frame is used.

7.1 Quadratic rotor current control with SMC

The sliding surface representing the error between the measured and reference quadratic rotor current is given by this relation:

$$e = {i_{rq}}^* - i_{rq} \quad (38)$$

For $n = 1$, the speed control manifold equation can be obtained from equation (37) as follow:

$$\sigma_s(i_rq) = e = {i_{rq}}^* - i_{rq} \quad (39)$$

$$\dot{\sigma}_s(i_{rq}) = \dot{i_{rq}}^* - \dot{i_{rq}} \tag{40}$$

Substituting the expression of $\dot{i_{rq}}$ equation (26) in equation (40), we obtain:

$$\begin{aligned}\dot{\sigma}(i_{rq}) =& \dot{i_{rq}}^* - \left(-\frac{1}{\sigma}\left(\frac{1}{T_r} + \frac{M^2}{L_S T_s L_r}\right) i_{rq} \right. \\ & \left. - g\omega_s i_{rd} + \frac{1}{\sigma L_r} V_{rq} \right)\end{aligned} \tag{41}$$

We take:

$$V_{rq} = V_{rq}^{eq} + V_{rq}^{n} \tag{42}$$

During the sliding mode and in permanent regime, we have:

$$\sigma_s(i_{rq}) = 0, \dot{\sigma_s}(i_{rq}) = 0, V_{rq}^{n} = 0 \tag{43}$$

Where the equivalent control is:

$$V_{rq}^{eq} = \left(\dot{i_{rq}}^* + \frac{1}{\sigma}\left(\frac{1}{T_r} + \frac{M^2}{L_S T_s L_r}\right) i_{rq} + g\omega_s i_{rd} \right) \sigma L_r \tag{44}$$

Therefore, the correction factor is given by:

$$V_{rq}^{n} = k_{V_{rq}} sat(\sigma_s(i_{rq})) \tag{45}$$

$k_{v_{rq}}$: positive constant.

7.2 Direct rotor current control with SMC

The sliding surface representing the error between the measured and reference direct rotor current is given by this relation:

$$e = {i_{rd}}^* - {i_{rd}}^* - i_{rd} \tag{46}$$

For $n = 1$, the speed control manifold equation can be obtained from equation (37) as follow:

$$\sigma_s(i_{rd}) = e = {i_{rd}}^* - i_{rd} \tag{47}$$

$$\dot{\sigma}_s(i_{rd}) = \dot{i_{rd}}^* - \dot{i_{rd}} \tag{48}$$

Substituting the expression of $\dot{i_{rd}}$ equation (25) in equation (48), we obtain:

$$\dot{\sigma_s}(i_{rd}) = \dot{i_{rd}}^* - \left(-\frac{1}{\sigma T_r} i_{rd} + g\omega_s i_{rq} + \frac{1}{\sigma L_r} V_{rd} \right) \tag{49}$$

We take:

$$V_{rd} = V_{rd}^{eq} + V_{rd}^{n} \tag{50}$$

During the sliding mode and in permanent regime, we have:

$$\sigma_s(i_{rd}) = 0, \dot{\sigma_s}(i_{rd}) = 0, V_{rd}^{n} = 0 \tag{51}$$

Where the equivalent control is:

$$V_{rd}^{eq} = \left(\dot{i_{rd}}^* + \frac{1}{\sigma T_r} i_{rd} - g\omega_s i_{rq} \right) \sigma L_r \tag{52}$$

Therefore, the correction factor is given by:

$$V_{rd}^{n} = k_{V_{rd}} sat(\sigma_s(i_{rd})) \tag{53}$$

$k_{V_{rd}}$: positive constant.

8. SIMULATION RESULTS

The complete control block diagram employing the sliding mode controller for stator active and reactive powers control is shown in Fig. 11. It shows the overall d-q vector control structure using the stator flux oriented frame using the sliding mode controller, the blocks represent the proposed sliding mode controllers of direct and quadratic rotor current. The block 'dq/abc' makes the conversion between the synchronously rotating and stationary reference frame. The block 'abc /dq' makes the inversion 'dq/abc' block. The block 'SVM' shows the control by technique space vector modulation whose is realized for the inverter control, which feeds the rotor through a converter. The block 'DFIG' represents the doubly fed induction generator coupled with wind turbine. The DFIG used in this work is a 4 kW, whose nominal parameters are indicated in appendix A. To verify the feasibility of the proposed control scheme, computer simulations were performed using Matlab/Simulink software. The block diagram was realized and executed on Intel Celeron PC having 2.5 GHz CPU, 1GB DDR RAM. In this section, simulation results are given to illustrate the system performance of the proposed SMC with SVM inverter schemes and compared with SMC with PWM inverter. The variation of wind speed is simulated in Fig. 12, the wind speed is start at 4m/s, at 2.5s, it suddenly changing at 5m/s, as 4s, it is 8 m/s. Fig. 13 shows the turbine rotor speed according the MPPT. After each variation of wind speed, the turbine rotor speed stables totally with the theoretical value. During this variation process, realize the maximum wind energy tracking control. Fig.14 shows the power coefficient variation C_p, it is kept around its maximum value $C_p = 5$. The Fig. 15 presents the stator active power and theirs reference profiles injected into the grid using two level inverter controlled by PWM and SVM technique. The stator reactive power and theirs reference profiles using PWM and SVM are presented in Fig.16. After the Fig.15 and Fig.16 a very good decoupling between the stator active and reactive powers is obtained in the two cases where used PWM and SVM technique. It is clear that the actual stator active power follows its desired values using the proposed controller incorporating PWM and SVM technique, and to guarantee a unity power factor at the stator side, the reactive power is maintained to zero. Ripples on active and reactive powers are reduced in SVM case where compared SVM with PWM as shown clearly in Fig.15 and Fig.16. Fig.17 and Fig 18 show stator current versus time using PWM and SVM respectively with theirs zoom. Fig.19 and Fig.20 present the rotor current of the DFIG using PWM and SVM respectively and theirs zoom. After Fig.17, Fig.18, Fig.19 and Fig.20, we observe that with when the wind speed increasing the amplitude of stator and rotor current increases. Fig.21 and Fig.22 show the harmonic spec-

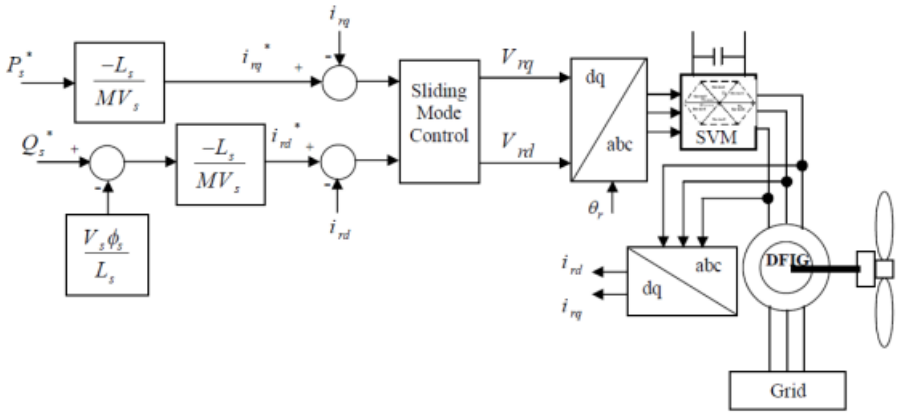

Fig.11: *Block diagram of SMC applied to the DFIG.*

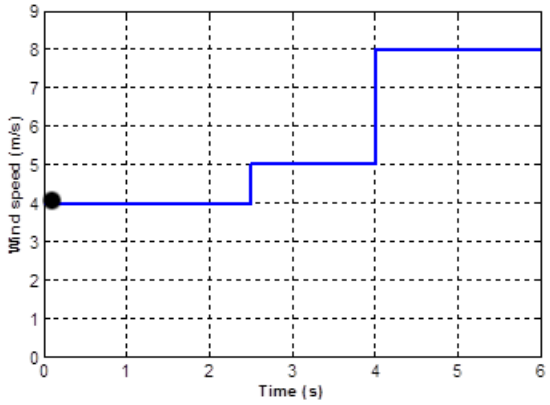

Fig.12: *Wind speed profiles.*

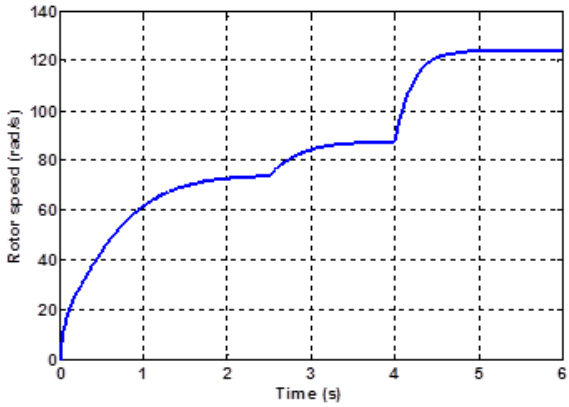

Fig.13: *Turbine rotor speed according the MPPT.*

trum of output phase stator and rotor current respectively obtained using Fast Fourier Transform (FFT) technique for PWM and SVM inverter. It can be clear observed that the most harmonics are eliminated in SVM case (THD calculated from the frequency spectrum is equal to 2.54% for stator current and 0.96% for rotor current "as shown in Fig.21.b and Fig.22.b"), compared to PWM case (THD equal to 6.62% for stator current and 2.49% for rotor current "as shown in Fig. 21.a and Fig. 22.a").

9. CONCLUSION

This paper presents simulation results of sliding mode control for active and reactive indirect power control of a DFIG, using the modulation strategy of the SVM compared with PWM technique. With results obtained from simulation, it is clear that for the same operation condition, the DFIG active and reactive power control with SMC using SVM technique had good performance than the PWM technique and that is clear in the spectrum of phase stator and rotor current harmonics which the use of the SVM, it is minimized of harmonics more than PWM technique. The performance of the DFIG can be further improved by minimizing the current harmonics in the stator and rotor current obtaining improved active and reactive power performance with reduced powers ripple.

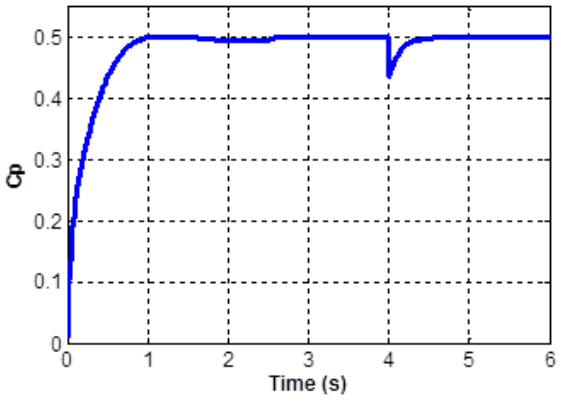

Fig.14: *Power coefficient C_p variation.*

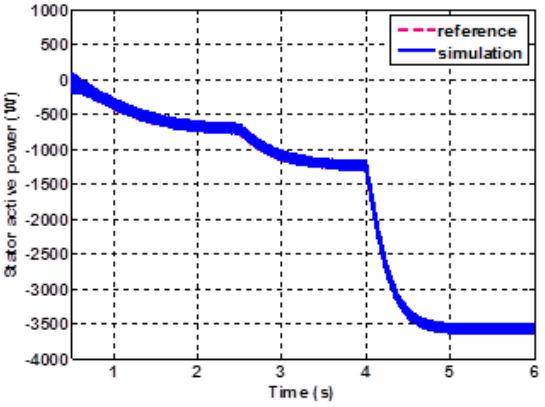

(a)

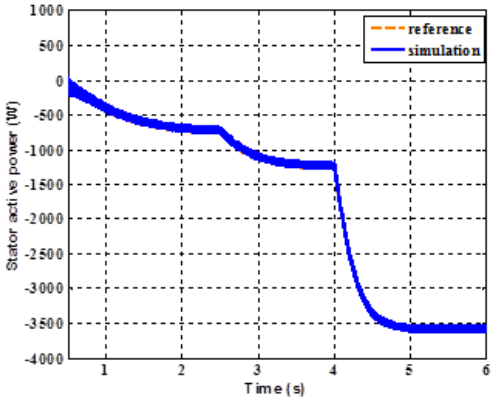

(b)

Fig.15: *Stator active power injected into the grid using: (a) PWM and (b) SVM.*

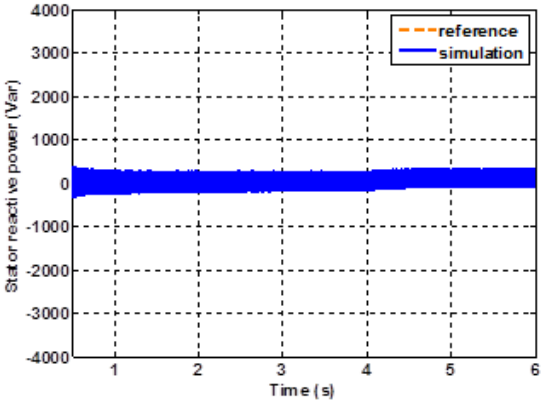

(a)

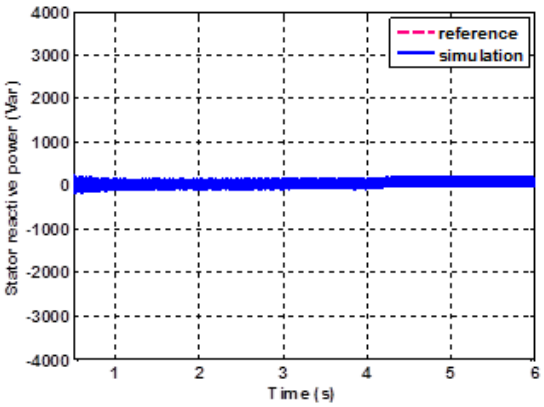

(b)

Fig.16: *Stator reactive power using: (a) PWM and (b) SVM.*

APPENDIX

Appendix I. System parameters.

DFIG data:

Rated values:
4 kW, 220/380 V, 50Hz, 15/8.6 A
Rated parameters:
$R_S = 1.2\Omega$
$R_r = 1.8\Omega$
$L_S = 0.1554H$
$M = 0.15H$
$P = 2$
Mechanical constants:
$J = 0.2Kg.m^2$
$f = 0.001N.m.s/rad$

Wind turbine data:

$R = 3m, G = 5.4, Numberofbleades = 3$

Air density value:

$\rho = 1.22Kg/m^3$

Appendix II. Nomenclature.

Turbine

Ω_{mec}	mechanical speed of the DFIG
Ω_t	turbine speed
P_t	turbine aerodynamic power
P_{m_ref}	reference mechanical power
C_p	power coefficient
C_{p_max}	maximum power coefficient
C_t	turbine torque
C_{em_ref}	reference electromagnetic torque
v	wind speed
v_{est}	estimated wind speed
λ	tip speed ratio
λ_{opt}	optimum tip speed ratio
β	pitch angle
R	blade length
G	gear box

DFIG

P_s, Q_s	active and reactive stator power
P_r, Q_r	active and reactive rotor power
$V_{sd}, V_{sq}, V_{rd}, V_{rq}$	stator and rotor d-q frame voltages

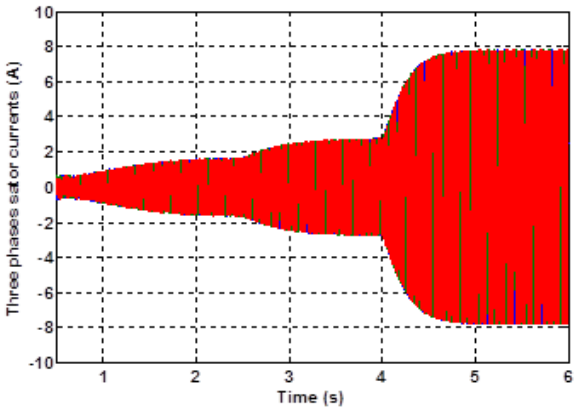

(a)

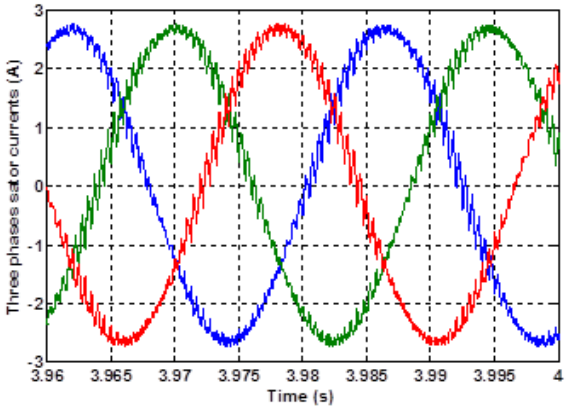

(b)

Fig.17: *(a) Stator current and (b) its zoom using PWM.*

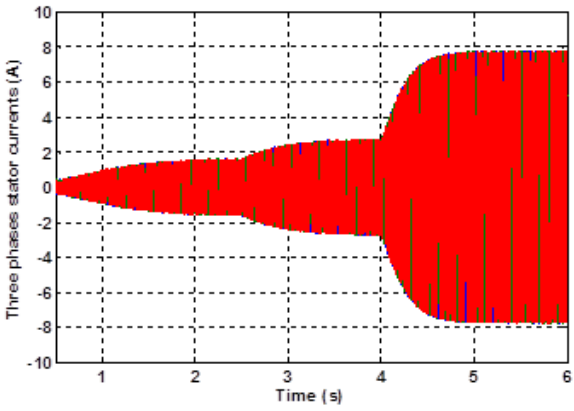

(a)

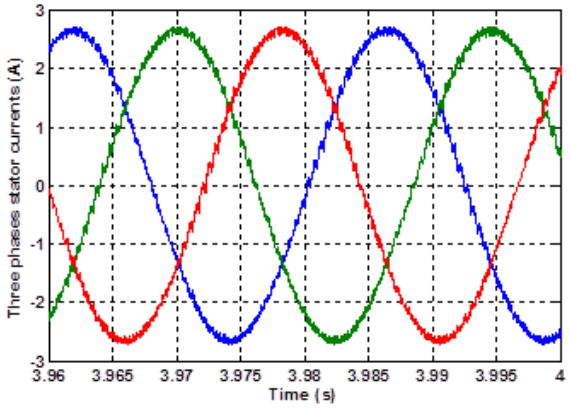

(b)

Fig.18: *(a) Stator current and (b) its zoom using SVM.*

$\phi_{sd}, \phi_{sq}, \phi_{rd}, \phi_{rq}$	stator and rotor d-q frame fluxes
R_s, R_r	stator and rotor resistances
L_s, L_r	stator and rotor inductances
M	mutual inductance
σ	leakage factor
T_s, T_r	statoric and rotoric time-constant
Ω	DFIG speed
C_e	electromagnetic torque
C_r	load torque
J	moment of inertia
f	friction coefficient
P	number of pole pairs
ω_s, ω	stator and rotor angular speed
g	slip coefficient
V_{DC}	direct current voltage

Sliding mode control

$S, \sigma_s(x,t)$	sliding surface
sgn	sign function
sat	saturation function
x	state vector
x_d	desired state vector
$[.]^T$	transposed vector
u	control vector
u^{eq}	equivalent control vector
u^n	switching part of the control
k_f	controller gain
e	error vector
τ	positive coefficient
n	system order
η	positive constant

Subscripts

d, q	synchronous d-q axis
s, r	stator, rotor

Acronyms

DFIM	Doubly Fed Induction Machine
DFIG	Doubly Fed Induction Generator
WECS	Wind Energy Conversion System
MPPT	Maximum Power Point Tracking
PWM	Pulse Width Modulation
SVM	Space Vector Modulation
SMC	Sliding Mode Control
THD	Total Harmonic Distortion

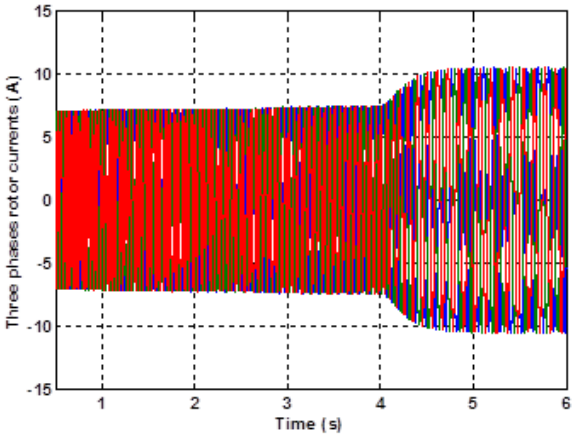

(a)

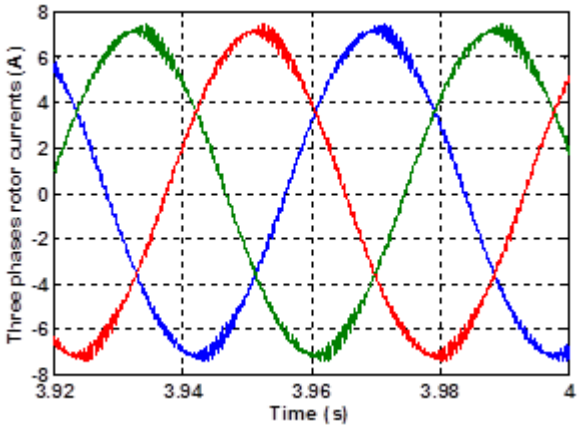

(b)

Fig.19: *(a) Rotor current and (b) its zoom using PWM.*

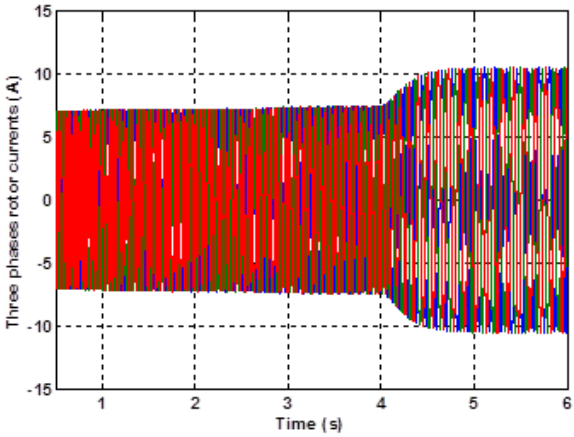

(a)

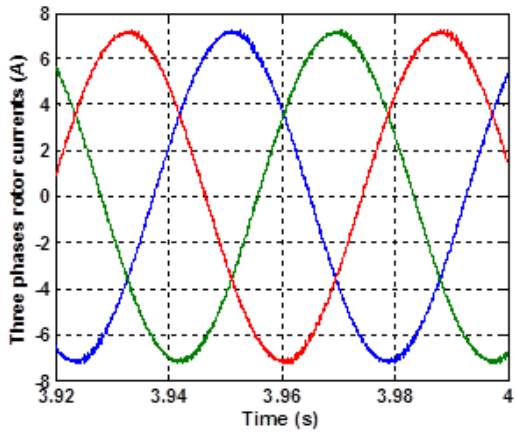

(b)

Fig.20: *(a) Rotor current and (b) its zoom using SVM.*

References

[1] A. Gaillard, P. Poure, S. Saadate, M. Machmoum, "Variable speed DFIG wind energy system for power generation and harmonic current mitigation," *Renewable Energy*, vol. 34, iss. 6, pp. 1545-1553, Jun. 2009.

[2] M. Verij Kazemi, A. Sadeghi Yazdankhah, H. Madadi Kojabadi, "Direct power control of DFIG based on discrete space vector modulation,"*Renewable Energy*, vol. 35, iss. 5, pp. 1033-1042, May 2010.

[3] WU Guo-qing, NI Hong-jun, WU Guo-xiang, ZHOU Jing-ling, Zhu Wei-nan, MAO Jing-feng, CAO Yang, "On maximum power point tracking control strategy for variable speed constant frequency wind power generation," *J. Chongqing University*, vol. 9, no. 1, pp. 21-28, Mar. 2010.

[4] A. Hazzab, I. K. Bousserhane, M. Kamli, M. Rahli, "Adaptive fuzzy PI-sliding mode controller for induction motor speed control," *Int. J. Emerging Electric Power Syst.*, vol. 4, no. 1, pp. 1-13, Nov. 2005.

[5] V. Katic, D. Graovac, "A method of real analysis of AC/DC converter line side harmonics," *Electronics and Energetics*, vol. 10, no. 1, pp. 107-123, month 1997.

[6] A. Jidin, T. Sutikno, "Matlab/simulink based analysis of voltage source inverter with space vector modulation," *TELKOMNIKA*, vol. 7, no. 1, pp. 23-30, Apr. 2009.

[7] D. Aouzellag, K. Ghedamsi, E.M. Berkouk, "Network power flux control of a wind generator," *Renewable Energy*, vol. 34, iss. 3, pp. 615-622, Mar. 2009.

[8] E. S. Abdin, W. Xu, "Control design and dynamic performance analysis of wind turbine-induction generator unit," *IEEE Trans. Energy Convers.*, vol. 15, no. 1, pp.91-96, Mar. 2000.

[9] Youcef Bekakra and Djilani Ben attous, "Active and reactive power control of a DFIG with MPPT for Variable Speed wind energy conversion using sliding mode control," *World Academy Sci., Eng. Technology*, vol. 60, pp. 1543-1549, Dec. 2011.

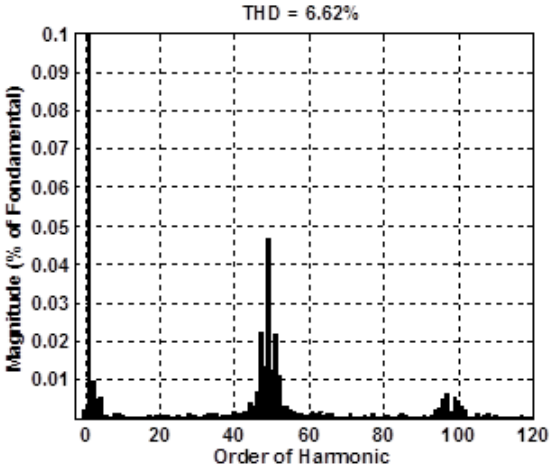

(a)

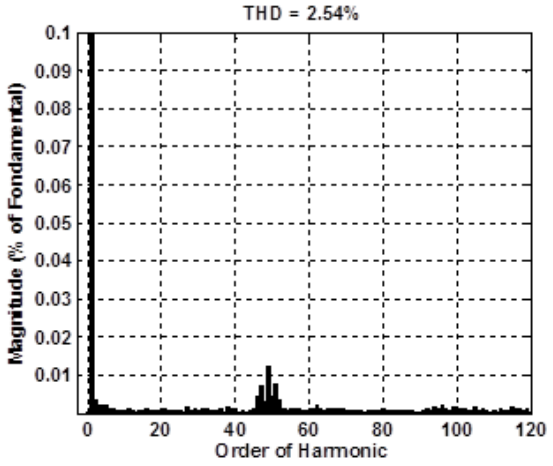

(b)

Fig.21: *Spectrum of phase stator current harmonics using: (a) PWM and (b) SVM.*

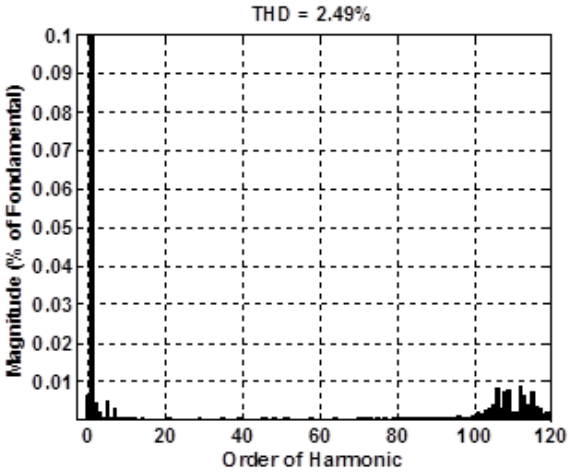

(a)

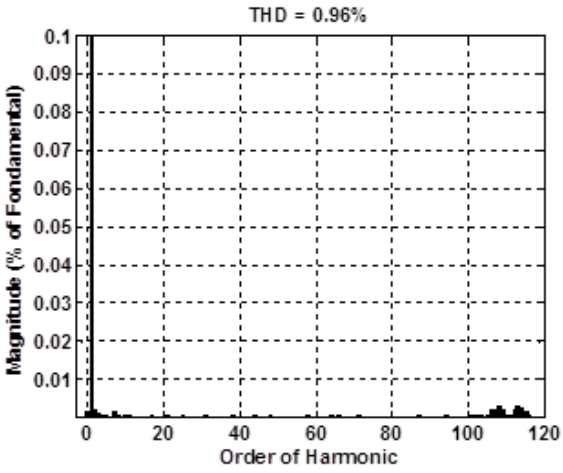

(b)

Fig.22: *Spectrum of phase rotor current harmonics using: (a) PWM and (b) SVM.*

[10] M. Machmoum, F. Poitiers, "Sliding mode control of a variable speed wind energy conversion system with DFIG," *Int. Conf. Exhibition Ecologic Vehicles and Renewable Energies*, Monaco, 2009, pp. 26-29.

[11] R. Arulmozhiyal, K. Baskaran, "Space vector pulse width modulation based speed control of induction motor using fuzzy PI controller," *Int. J. Comput. and Elect. Eng.*, vol. 1, no. 1, pp.98-103, Apr. 2009.

[12] A. Savulescu, "A spects of variable speed control of asynchronous motors through the technique of space vector modulation," *6th Int. Conf. Electromechanical Power Syst.*, Chisinau, Moldova, 2007, pp. 43-46.

[13] A. Savulescu, "The analysis and the simulation of the SVM generator used for the control of the electric drives with asynchronous motors," *6th Int. Conf. Electromechanical Power Syst.*, Chisinau, Moldova, 2007, pp. 47-50.

[14] A. Nasri, A. Hazzab, I. K. Bousserhane, S. Hadjiri, P. Sicard, "Two wheel speed robust sliding mode control for electrical vehicle drive," *Serbian J. Elect. Eng.*, vol. 5, no. 2, pp. 199-216, Nov. 2008.

[15] Y. Bekakra, D. Ben attous, A sliding mode speed and flux control of a doubly fed induction machine, *6th Int. Nat. Elect. Electron. Eng.*, Bursa, Turkey, 2009, pp. I-174 - I-178.

[16] M. Abid, A. Mansouri, A. Aissaoui, B. Belabbes, "Sliding mode application in position control of an induction machine," *J. Electron. Eng.*, vol. 59, no. 6, pp.322-327, Dec. 2008.

[17] J. Lo, Y. Kuo, "Decoupled fuzzy sliding mode control," *IEEE Trans. Fuzzy Syst.*, vol. 6, no. 3, pp. 426-435, Jun. 1998.

Youcef BEKAKRA was born in El-Oued, Algeria in 1984. He received the B.Sc degree in Electrical Engineering from El-Oued University, Algeria in 2007, his MSc degree from El-Oued University in 2010. He is currently working towards his PhD degree in Electrical Engineering from Biskra University, Algeria. His areas of interest are renewable energy, Electrical Drives and Process Control, application of Artificial Intelligence techniques for control and optimize electric power systems.

Djilani BEN ATTOUS was born in El-Oued, Algeria in 1959. He received his Engineer degree in Electrotechnics from Polytechnic National Institute Algiers, Algeria in 1984. He got MSc degree in Power Systems from UMIST England in 1987. In 2000, he received his doctorate of state (PhD degree) from Batna University, Algeria. He is currently associate professor at El-Oued University, Algeria in Electrical Engineering. His research interests in Planning and Economic of Electric Energy System, Optimization Theory and its applications and he also investigated questions related with Electrical Drives and Process Control. He is member of the VTRS research Laboratory.